Journal of Power Sources 228 (2013) 97–103

Contents lists available at SciVerse ScienceDirect

Journal of Power Sources

journal homepage: www.elsevier.com/locate/jpowsour

Short communication

Structural optimization of (La, Sr)CoO_3-based multilayered composite cathode for solid-oxide fuel cells

Sun-Young Park, Ho-Il Ji, Hae-Ryoung Kim, Kyung Joong Yoon, Ji-Won Son, Byung-Kook Kim, Hae-Jun Je, Hae-Weon Lee, Jong-Ho Lee*

High-temperature Energy Materials Research Center, Korea Institute of Science and Technology, Seoul 136-791, Republic of Korea

HIGHLIGHTS

- Compositional effects of the cathode on unit-cell performance are investigated.
- $La_{0.6}Sr_{0.4}CoO_3$ is more effective for increasing the electrocatalytic activation.
- $La_{0.6}Sr_{0.4}CoO_3$ is more effective for cathode current collection.
- Well-designed architecture for cathode is essential for high cell performance.

ARTICLE INFO

Article history:
Received 12 October 2012
Received in revised form
19 November 2012
Accepted 20 November 2012
Available online 29 November 2012

Keywords:
Lanthanum strontium cobaltite
Solid-oxide fuel cell
Cathode functional layer
Cathode-current-collecting layer
Oxygen reduction reaction

ABSTRACT

In the present study, (La, Sr)CoO_3 material was screen-printed as a cathode and as current-collecting layers for planar-type low-temperature solid-oxide fuel cells (SOFCs). The compositional effects of the cathode functional and current-collecting layer on unit-cell performance were investigated using AC and DC polarization experiments. Two different cathode (La, Sr)CoO_3 materials, $La_{0.6}Sr_{0.4}CoO_3$ and $La_{0.8}Sr_{0.2}CoO_3$, were examined, and $La_{0.6}Sr_{0.4}CoO_3$ was found to be more effective for increasing the electrocatalytic activation and collection efficiency of the current produced in the cathode reaction. Furthermore, a well-designed architecture for the current-collecting layer was very effective in increasing unit-cell performance by reducing the contact resistance between SOFC cathodes and interconnects.

1. Introduction

Numerous studies have shown that cathode polarization is the major contributor to overall performance losses in Solid-oxide fuel cells (SOFCs) [1–5]. Thus current research focus has shifted toward the development of new cathode materials that offer good electrochemical performance at the temperature substantially below 800 °C. In particular, mixed ionic and electronic conducting (MIEC) perovskites such as ABO_3-structured cobaltites and ferrites are promising candidates for such materials [6–8]. For most of the perovskite materials used as cathodes in SOFCs, the A-site cation is a mixture of rare and alkaline earths (such as La and Sr, Ca, or Ba), while the B-site cation is a reducible transition metal such as Mn, Fe, Co, or Ni. Thus in most cases, a redox catalytic mechanism is usually provided by B-site cations. [9] The octahedral symmetry around the transition metal, on the other hand, often promotes a metallic or semiconducting band structure at high temperatures, leading to high electronic conduction.

Perovskite-structured strontium-substituted lanthanum cobalt oxides ($La_{1-x}Sr_xCoO_{3-\delta}$) have attracted great scientific and technical interest because of their versatile characteristics, such as spin-state-associated magnetic behavior [10,11], high oxidation catalytic activity [12,13], and excellent oxygen electrode performance [14,15]. Specifically, the substantial electrode activity of $La_{1-x}Sr_xCoO_{3-\delta}$ (LSC) is mainly due to high oxygen diffusivity and high dissociation ability of oxygen molecules [14]. Moreover, most cobalt-based perovskite materials display higher ionic and electronic conductivities than other cathode materials, so the use of cobalt-containing cathode materials should result in a decreased cathode polarization resistance. However, using a large amount of cobalt results in an increased thermal expansion coefficient (TEC), which may in turn result in delamination at the cathode/electrolyte

* Corresponding author. Tel.: +82 2 958 5532; fax: +82 2 958 5529.
E-mail address: jongho@kist.re.kr (J.-H. Lee).

0378-7753/$ – see front matter © 2012 Elsevier B.V. All rights reserved.
http://dx.doi.org/10.1016/j.jpowsour.2012.11.108

interface or electrolyte cracking due to the large degree of TEC mismatch between the cathode and the electrolyte [16]. Besides this disadvantage, cobaltite cathodes react readily with yttria-stabilized zirconia (YSZ) to form insulating compounds during sintering, which significantly degrades cathode performance. Thus, a diffusion barrier layer is usually used for cells consisting of cobaltite-based cathodes and the YSZ electrolyte [17,18].

In general, the physicochemical properties of $La_{1-x}Sr_xCoO_{3-\delta}$ can be changed by varying its Sr content. According to previous research, the oxygen non-stoichiometry (δ) of LSC increases with increasing Sr content [19–21], and, consequently, the thermal expansion coefficient (TEC) and ionic conductivity of LSC also increase [19,22,23]. However, the total LSC electrical conductivity initially increases to $x = 0.5$ and then decreases because of the charge compensation associated with hole consumption at higher Sr contents [21]. Thus, high Sr content is detrimental to total electrical conductivity while simultaneously being advantageous to LSC ionic conductivity. Moreover, considering that the TECs of SOFC electrolyte materials, such as doped zirconia and ceria, are much lower than those of cathodes [24], high-Sr-content LSC is unsuitable for solving the delamination problem due to TEC mismatch. Hence, a tradeoff between increasing electrochemical performance and decreasing thermal expansion may be necessary to achieve optimal cathode composition.

Another strategy for solving the delamination problem is to use the porous LSC/electrolyte composite material usually used in practical SOFC cathodes. This porous cathode composite has fairly excellent electrocatalytic activity for oxygen reduction reaction and has desirable thermomechanical and chemical compatibilities with conventional electrolytes. However, the relatively low electronic conductivity of the composite material is supposed to impede the lateral distribution of the electrical flux, deteriorating current-collecting efficiency during cell operation. Thus, an additional cathode-current-collecting layer (CCCL) is usually necessary on top of this cathode composite layer [25–27].

In this study, two (La, Sr)CoO_3-based materials with different Sr compositions, $La_{0.6}Sr_{0.4}CoO_3$ (LSC64) and $La_{0.8}Sr_{0.2}CoO_3$ (LSC82), were examined as candidates for cathode and current-collecting materials. We used each of them as a composite cathode functional layer (CFL) consolidated with $Gd_{0.1}Ce_{0.9}O_{1.95}$ (GDC, Rhodia, USA) and also as a CCCL in monolithic form. The compositional effects and their complex contribution to both electrical and electrochemical properties of CFL and CCCL were investigated using unit- and half-cell tests. The correlation of LSC composition and the corresponding physicochemical properties with consequential electrochemical performance of SOFCs were also investigated.

2. Experimental

2.1. Fabrication of unit- and half-cells

Commercial YSZ (Tosho, Japan) and nickel oxide (NiO, Sumitomo, Japan) powders were used to prepare NiO-YSZ anode substrates. NiO-YSZ composite powder granules were pressed into a green anode substrate. An anode functional layer (AFL) having the same composition with the anode substrate but without having coarse-grained YSZ powder was screen-printed onto the NiO-YSZ substrate. A 1 m/o Al_2O_3-doped 10 m/o Sc_2O_3–ZrO_2 (SEIMI, Japan) electrolyte layer was also screen-printed onto the AFL and co-sintered at 1400 °C. A GDC blocking layer was then screen-printed onto the co-fired anode/electrolyte layer to prevent interfacial reaction between the zirconia-based electrolyte and LSC-based cathode, which is very detrimental to SOFC performance. The GDC blocking layer was then sintered at 1250 °C where undesirable interfacial reaction between YSZ and GDC can be suppressed. For the CFL, we used two LSC powders with different Sr compositions, LSC64 and LSC82 (AGC SEMI, Japan), which have very different catalytic and electrical properties. A composite CFL (LSC:GDC = 50:50 wt%) was screen-printed onto the GDC layer to diminish the degree of thermomechanical mismatch between the LSC-based cathode and the GDC blocking layer. An additional single-phase LSC-based CCCL was screen-printed onto the LSC–GDC CFL and was then co-fired at 950 °C. The fabrication conditions for the differently configured LSC cathode-based 10 × 10 cm^2 unit cells are summarized in Tables 1 and 2. GDC powder was compacted into disk-shaped pellets that were sintered at 1500 °C in air to produce the half-cells. Similarly configured LSC–GDC CFLs and LSC CCCLs were constructed on both sides of dense (0.7 mm thick, 8.1 mm in diameter) GDC pellets by using screen-printing. The pellets were then co-fired at 950 °C: the same condition under which the cathode of unit cell was sintered.

2.2. Characterization of unit- and half-cells

The effects of a CCCL were investigated by comparing the performance of unit cells with and without the additional LSC-based CCCL (Table 1). To compare the difference in current-collecting efficiency of the unit cells, we used the same LSC64-based CFL. We also differentiated between current-collecting efficiencies on the basis of different CCCL fabrication procedures: LSC6464 and LSC64 + 64 were fabricated by co- and sequential sintering with CFL, respectively, which was expected to cause different microstructural features, such as porosity and interfacial bonding between CFL and CCCL, in the different unit cells. Further, the effects that LSC composition had on the cathodic and current-collecting efficiency of the unit cells were investigated by changing the LSC composition of the CFL and CCCL (Table 2). These differences in double-layered cathode configurations were also characterized for symmetric half-cells having the same cathode structure on both sides of the electrolyte pellet. A ceramic–glass composite sealant and an Inconel®-based metallic interconnect (25 channels and 24 ribs on each cathode and anode side) were used for measuring unit-cell performance. The flow channels of the cell testing unit were designed to have co-flowing fuel gas and air. The current–voltage and current–power characteristics were measured using an SOFC test station (SAT890C, Toyo., Japan) in the range 650–750 °C. Air was used as the oxidant, and moisturized hydrogen (H_2 + 3%

Table 1
Summary of fabrication conditions for unit cells used for investigating effects of LSC composition in CCCL (AFL: anode functional layer, CFL: cathode functional layer, CCCL: cathode-current-collecting layer).

Cell notation and configuration	Anode substrate	AFL	Electrolyte	Blocking layer	CFL	CCCL
LSC64 cell	NiO-YSZ	NiO-YSZ	Al-ScSZ	GDC	LSC–GDC ($La_{0.6}Sr_{0.4}CoO_3$)	X
	$1.5 < x < 3.0$ mm	~15 μm	~8 μm	~6 μm	~24 μm	X
LSC64 + 64 cell	NiO-YSZ	NiO-YSZ	Al-ScSZ	GDC	LSC–GDC ($La_{0.6}Sr_{0.4}CoO_3$)	$La_{0.6}Sr_{0.4}CoO_3$
	$1.5 < x < 3.0$ mm	~15 μm	~8 μm	~6 μm	~24 μm	~12 μm
LSC6464 cell	NiO-YSZ	NiO-YSZ	Al-ScSZ	GDC	LSC–GDC ($La_{0.6}Sr_{0.4}CoO_3$)	$La_{0.6}Sr_{0.4}CoO_3$
	$1.5 < x < 3.0$ mm	~15 μm	~8 μm	~6 μm	~16 μm	~15 μm

Table 2
Summary of fabrication conditions for unit cells used for investigating effects of LSC composition in cathodes (AFL: anode functional layer, CFL: cathode functional layer, CCCL: cathode-current-collecting layer).

Cell notation and configuration	Anode substrate	AFL	Electrolyte	Blocking layer	CFL	CCCL
LSC6464 cell	NiO-YSZ $1.5 < x < 3.0$ mm	NiO-YSZ ~15 μm	Al-ScSZ ~8 μm	GDC ~6 μm	LSC–GDC ($La_{0.6}Sr_{0.4}CoO_3$) ~16 μm	$La_{0.6}Sr_{0.4}CoO_3$ ~15 μm
LSC8282 cell	NiO-YSZ $1.5 < x < 3.0$ mm	NiO-YSZ ~15 μm	Al-ScSZ ~8 μm	GDC ~6 μm	LSC–GDC ($La_{0.8}Sr_{0.2}CoO_3$) ~15 μm	$La_{0.8}Sr_{0.2}CoO_3$ ~10 μm
LSC8264 cell	NiO-YSZ $1.5 < x < 3.0$ mm	NiO-YSZ ~15 μm	Al-ScSZ ~8 μm	GDC ~6 μm	LSC–GDC ($La_{0.8}Sr_{0.2}CoO_3$) ~15 μm	$La_{0.6}Sr_{0.4}CoO_3$ ~10 μm

H_2O) was used as fuel. The cell area-specific resistance (ASR) was calculated at open circuit voltage (OCV). Electrochemical impedance was also measured using a frequency response analyzer (SI 1260, Solartron Analytical) combined with an electrochemical interface (SI1287, Solartron Analytical). Each impedance spectrum (IS) was recorded in the range 10 MHz–0.1 Hz and was generated as both Nyquist and Bode plots for comparison. The electrode microstructures of the cells were analyzed post mortem by using scanning electron microscopy (SEM, Hitachi S-4200) after performance characterization.

3. Results and discussion

3.1. Half-cell tests

Fig. 1 shows the IS as Nyquist plots for the LSC82- and LSC64-based half-cells, measured using quasi-4-probe AC impedance spectroscopy. The pure polarization resistance component of both the LSC82- and LSC64-based half-cells were compared by subtracting the high-frequency intercepts, including the contribution of the ohmic resistance of the GDC electrolyte of half-cell. Fig. 1(a)

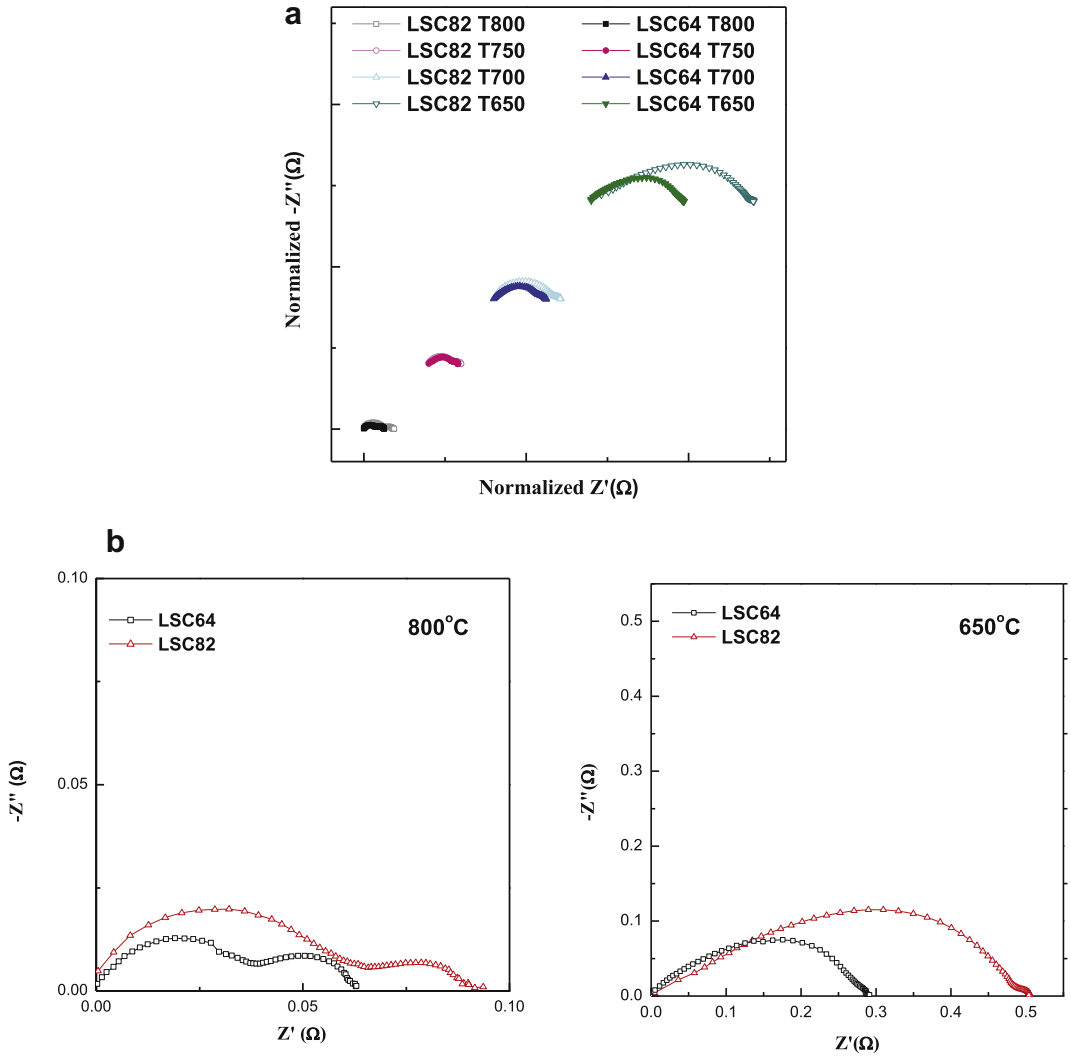

Fig. 1. AC impedance spectra measured for differently configured LSC-based cathode half-cells. (a) Comparison of LSC64- and LSC82-based half-cell impedances measured at various temperatures after subtracting ohmic contribution. (b) Comparison between LSC64- and LSC82-based half-cell impedances measured at 800 and 650 °C in air.

clearly shows that the polarization resistances of the LSC82 cathodes were always higher than those of the LSC64 cathodes regardless of operating temperature, indicating higher electrocatalytic activity for the LSC64 cathodes than that for the LSC82 cathodes. Although the absolute values of polarization resistance are different, the IS for both cells appear very similar with two to three impedance arcs each (depending on the operating temperature). Fig. 1(b) depicts the IS measurements for both samples measured at high (800 °C) and low (650 °C) temperatures, respectively. The IS measured at 800 °C displayed two impedance arcs: a high-frequency arc (1st arc, R2-CPE1) and low-frequency arc (2nd arc, R3-CPE2). However, in the IS measured at 650 °C, the high-frequency arc consists of numerous arcs, which could not be deconvoluted using conventional fitting methods. Hence the IS measurements in the present study were analyzed using an equivalent circuit composed of one resistance component (R1: high-frequency intercepts on the real axes in the original IS) and two serial resistance/constant phase element (R/CPE) parallel components (R-R/CPE-R/CPE).

The impedance arcs observed in the present study were analyzed in a systematic order. First, the high-frequency intercepts on the real axes in the original IS measurements (figure not shown here for brevity) for the LSC82 and LSC64 half-cells are attributed to the resistance of the GDC electrolyte disk ($R1$) of half-cell. The $R1$ values were obtained using the equivalent circuit fitting of the original IS measurements. According to the fitting results, the $R1$ values for both samples were almost identical and consistent with that expected for GDC electrolyte since the specific geometries of the GDC disks in both cells were maintained almost similar. Furthermore, the activation energies of the LSC82- and LSC64-based half-cells (0.607 and 0.592 eV, respectively) were fairly consistent despite being slightly lower than data in the literature [28], suggesting that attributing $R1$ to resistance associated with the GDC disks was valid.

When we re-examined Fig. 1(b), the two remaining impedance arcs were attributed to cathodic polarization losses for ORR at LSC-based cathodes. In general, an LSC-based mixed conducting cathode can follow three possible cathodic reaction paths: through electrode surface, bulk, and electrolyte surface [29]. Among them, the electrode bulk path can easily be followed by an LSC-based cathode because the MIEC property of LSC exhibits facile bulk oxygen transport via the vacancy mechanism [29]. One or more elementary steps in reaction pathways generally determine(s) the reaction rate of corresponding cathodic reaction path. Predicting which elementary reaction is the rate-limiting step is not always possible since local conditions, such as operating temperature, oxygen partial pressure, and/or microstructural anomalies, play vital roles in determining the rate-limiting step.

In real SOFCs where composite cathodes such as LSC–GDC are used, proper microstructural architecture plays a critical role in achieving a high performance from the cathode. Since the ORR within the porous cathode composite structure is closely associated with generation and transport of oxygen ions at or near the cathodic reaction site, [8] a higher population density of active reaction sites is essential for high performance cathodes. Since ORR can occur at the whole surface of the MIEC LSC phase among the LSC–GDC composites, enlarged surface area of the cathode composite plays a key role in improving cathode performance by leading more active sites for ORR. The importance of the surface area effect for the ORR rate for LSC electrodes has previously been reported by Endo et al. [30] as well.

ORR in MIEC LSC generally proceeds in the following sequence: (1) oxygen adsorption with dissociation, (2) ionization of oxygen by reduction, (3) incorporation of oxygen ions into the cathode surface, (4) bulk diffusion or surface diffusion of the oxygen ions, and (5) oxygen ion transfer through the cathode/electrolyte interface [31,32]. Among them, step (3) [32] or (4) [31,33] has generally been appeared as the main rate-limiting step for LSC, especially at compositions $La_{1-x}Sr_xCoO_3$ ($0.2 \leq x \leq 0.5$). The Bode plots of each IS for the LSC64- and LSC82-based half-cells were investigated to identify the dominant electrochemical processes in the ORR sequence since each reaction step of ORR has its own characteristic frequency region [34,35]. Fig. 2 shows the Bode plots of the IS for the (a) LSC64- and (b) LSC82-based half-cells measured in the range 650–800 °C. The LSC82-based half-cell has higher impedance values than the LSC64-based half-cell over the whole temperature range. In addition, the impedance value of the LSC82-based half-cell increases more rapidly with decreasing temperature than that of the LSC64-based half-cell, indicating that the activation energy of ORR in the LSC82-based half-cell is larger than that of ORR in the LSC64-based half-cell.

According to the literature on the analyzed characteristic frequency regions of ORR in LSC [36–38], step (5) usually appears in a high-frequency region around 10–100 kHz, whereas steps (1–4), corresponding to oxygen ion diffusion and oxygen surface exchange, appears in an intermediate frequency region of 10 Hz–10 kHz. In addition, out of the aforementioned ORR steps that occur at the LSC surface, oxygen gas diffusion through the porous cathode structure can also impede ORR, and it appears in the lower frequency region below 10 Hz. The Bode plot shows that two apparent frequency components can be considered for identifying the main rate-limiting step of ORR in the LSC–GDC cathode. Based on the aforementioned general classification criteria with respect to the characteristic frequency region, it is reasonable to attribute the larger impedance arc (1st arc, R2-CPE1) shown in Figs. 1 and 2 to an intermediate frequency component (10 Hz–10 kHz) and the smaller impedance arc (2nd arc, R3-CPE2) to a low-frequency component (<10 Hz), respectively. Hence, it can be anticipated

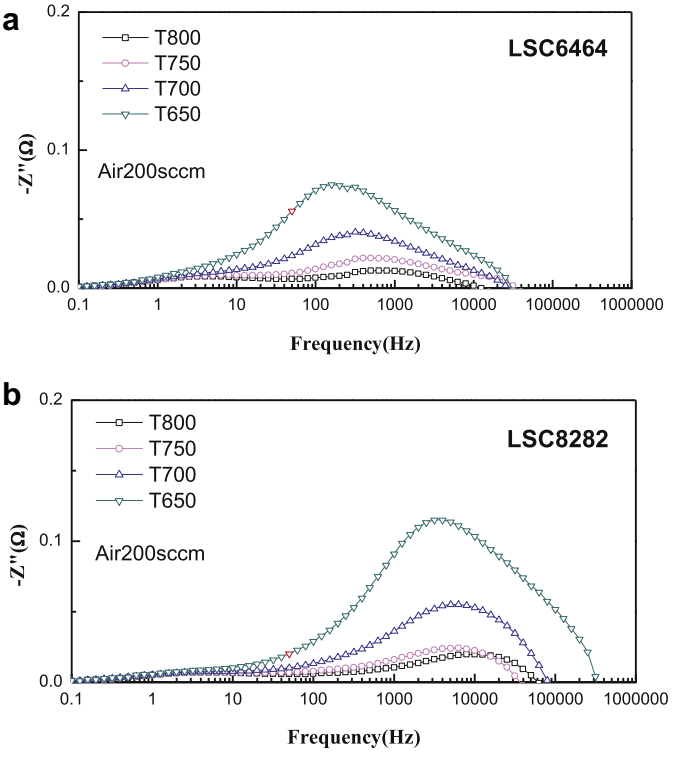

Fig. 2. Bode plots for comparison of LSC64- and LSC82-based half-cell impedances measured at various temperatures for (a) LSC64 and (b) LSC82.

that the relatively high-frequency component in total impedance spectra is due to the impedance associated with oxygen ion diffusion or/and oxygen surface exchange steps, whereas the low-frequency component is due to the limited gas phase diffusion through the porous cathode even though this assignment for low-frequency component is still debatable by considering the small amount of induced oxygen flux during the IS measurement. Nevertheless, on the basis of aforementioned categorization, it can be concluded that the major limiting step of ORR in the LSC–GDC cathode is associated with oxygen ion diffusion or/and oxygen surface exchange. The larger impedance associated with oxygen ion diffusion and oxygen surface exchange in the LSC82 cathode can be simply understood by the higher δ value for LSC64 because the kinetic properties of LSC are apparently proportional to the bulk oxygen vacancy concentration (δ) [32,33]. From a defect chemistry viewpoint, large-scale substitution of lower valence La with higher valence Sr in LSC64 induces higher δ, thereby leading to increased surface oxygen exchange and bulk oxygen diffusion [32,33].

The effects that temperature change had on these half-cells were investigated to further classify the intermediate frequency component (1st arc, R2-CPE in Figs. 1 and 2). The intermediate frequency component of the LSC82-based half-cell increases drastically with decreasing operating temperature, indicating that ORR is more temperature dependent in the LSC82 half-cell than it is in the LSC64 one. According to Lu et al., [33] with the changing temperature, the oxygen vacancy diffusivity (D_v) of both the LSC64 and LSC82 samples changed very little, whereas the surface exchange rate (K_0), especially of LSC82 changed more rapidly than that of LSC64. Hence, it can be postulated that the major limiting step of ORR in an LSC-based cathode is associated with oxygen surface exchange rather than with oxygen ion diffusion.

As previously mentioned, the surface exchange coefficient is apparently proportional to the bulk oxygen vacancy concentration, suggesting that oxygen vacancies are the active sites for surface reaction. Kilner et al. [39] thoroughly reviewed the role of oxygen vacancies and proposed an empirical relationship between the surface exchange coefficient, k, and the oxygen diffusion coefficient. They demonstrated that the oxygen vacancy concentration plays an important role in the surface exchange reaction. Hence, the difference in LSC64 and LSC82 performance originates from the difference in their respective Sr contents, and more precisely, from the difference in the number of oxygen vacancies generated by the addition of Sr.

3.2. Effects of cathode-current-collecting layer (CCCL) on unit-cell performance

Addition of a CCCL was very necessary to enhance the current-collecting efficiency of the composite cathode. (Usually composite cathodes will have a lower electrical conductivity than single phase cathodes.) In order to investigate the effects that a CCCL had on the electrochemical performance of the LSC–GDC composite cathodes, three differently configured LSC cathode-based 10 × 10 cm^2 unit cells were fabricated (Table 1), and their power generating capabilities were systematically characterized. From Fig. 3, the electrochemical performance of LSC64 cell without the CCCL was significantly lower than that of the cells with the CCCL (LSC6464, LSC64 + 64). Such a low electrochemical performance in the LSC64 cell without the CCCL can be explained by the inferior current-collecting efficiency of the LSC–GDC composite layer. The results of the AC impedance analysis shown in Fig. 4 indicate that the higher ohmic resistance of the LSC64 cell can be attributed to the increased amount of interfacial contact resistance originating from the absence of the CCCL. Once the CCCL is formed on a cathode, on the other hand, the fabrication history of the CCCL does not significantly affect the electrochemical performance of the cathode. As shown in Fig. 3, the LSC6464 cell (CCCL co-fired with CFL) shows a very slightly higher performance than the LSC64 + 64 cell, indicating that the microstructural properties of both cathodes are not significantly different despite their different fabrication histories. As shown in Fig. 4, the IS of the LSC6464 and LSC64 + 64 cells consists of two impedance arcs: a large high-frequency impedance arc ($f_{peak} \approx 100$ Hz) and a relatively smaller low-frequency impedance arc ($f_{peak} \approx 1.5$ Hz). It is interesting to note that, when the IS for the unit-cell tests are compared with those for the half-cell tests, the low-frequency component for the unit-cell tests is relatively larger than that for half-cell tests. By varying both the amount of fuel and oxidant gas flow, this low-frequency component was found to originate from the anode rather than from the cathode. This finding is further supported by the fact that no changes in the magnitude of the low-frequency component were found for the other cathode configurations. Hence, the high-

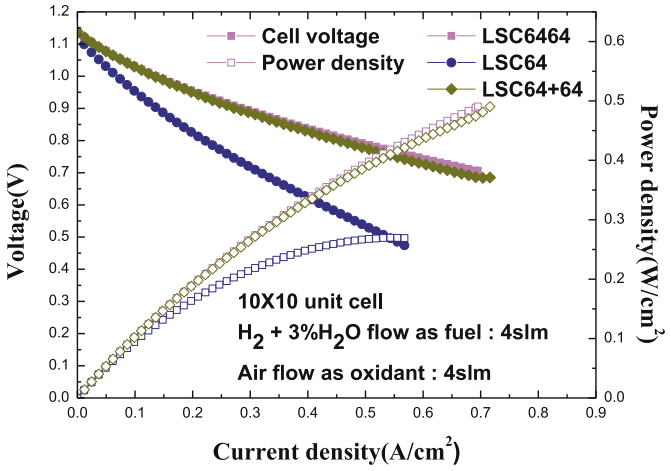

Fig. 3. Comparison of electrochemical performances of three differently configured 10 × 10 cm^2 unit cells with LSC-based CCCLs (670 °C).

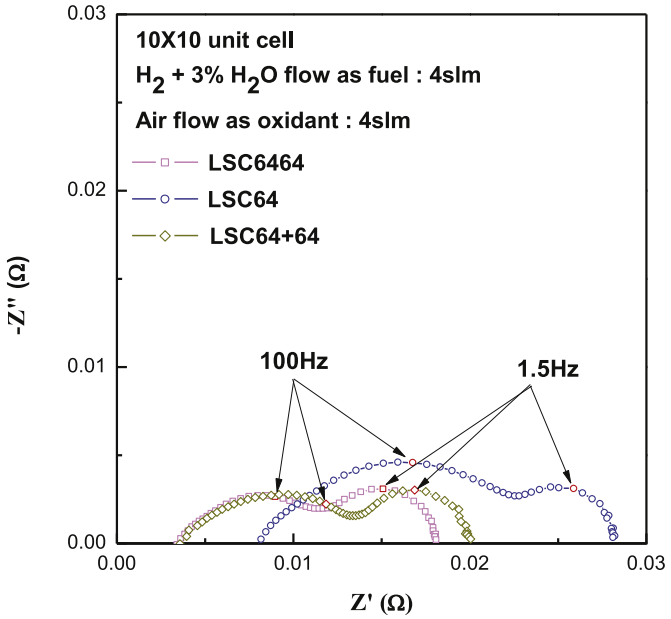

Fig. 4. Comparison of AC impedance spectra for with three differently configured 10 × 10 cm^2 unit cells with LSC-based CCCLs (670 °C, OCV condition).

frequency component of IS can be attributed to the cathodic polarization resistance. Nevertheless, as shown in Fig. 4, the high-frequency component of the LSC6464 cell is smaller than that of the LSC64 + 64 cell. Although the issue was not clearly resolved from SEM observations, this result suggests that some subtle differences in cell microstructural features induced such small differences in the cathodic polarization. In the current stage, the differences are probably due to some variations in the CFL microstructural evolution or to interfacial adhesion between the CFL and the CCCL, which can be altered by using different heat treatment conditions for the LSC6464 and LSC64 + 64 cells. From all these results taken together, the main differences in the power generation characteristics of three types of unit cells are mostly attributed to the presence or absence of the CCCL, which seems to change the current-collecting efficiency and eventually determines the contact resistance of a cathode with a metallic interconnector.

3.3. Effects of LSC composition on unit-cell performance

The effects that LSC composition had on the electrochemical performance of the LSC–GDC composite cathodes were investigated by fabricating three differently configured LSC64- or LSC82-based cathodes on 10 × 10 cm^2 unit cells (Table 2) and by characterizing their power generating capabilities. As shown in Table 2, the CFL and CCCL of the LSC6464 and LSC8282 cells were composed of the LSC64- and LSC82-based materials, respectively, while those of LSC8264 cell had LSC82-based CFL and LSC64-based CCCL cathode layers. The LSC8264 cell was designed to check the combined effect of the highly conductive LSC64-based CCCL with the less active LSC82-based CFL. The cross-sectional SEM images of these three different cells are shown in Fig. 5. The microstructural features of the unit cells, including the thickness of all constituent layers, were maintained such that electrochemical performance could primarily controlled by the physico-chemical nature of constituent materials rather than by the microstructural features of the CFL and CCCL.

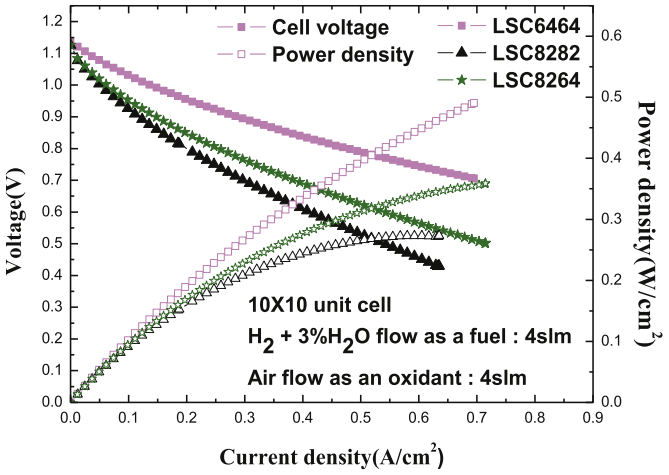

Fig. 6. Comparison of electrochemical performances of three differently configured 10 × 10 cm^2 LSC-based cathode unit cells (670 °C).

The electrochemical performances of these three different cells are compared in Fig. 6. The electrochemical performance was highest for the LSC6464 cell that had the LSC64-based CFL and CCCL. The electrochemical performances of the cells as arranged in descending order are as follows: LSC6464 > LSC8264 > LSC8282. These results are consistent with the previous half-cell test results showing that the LSC64 cell had a higher degree of electrochemical activity than the LSC82 cell. Because of the high electrical conductivity of LSC64, the LSC64-based CCCL should also have high current-collecting efficiency. On the basis of the high electrochemical activity and current-collecting efficiency of the LSC64-based material, the LSC6464 cell should show high cell performance. A poor cell performance is expected for the LSC8282 cell because of the inferior electrochemical activity and current-collecting efficiency of the LSC82-based material. A mid-level performance is expected for the LSC8264 cell because it is

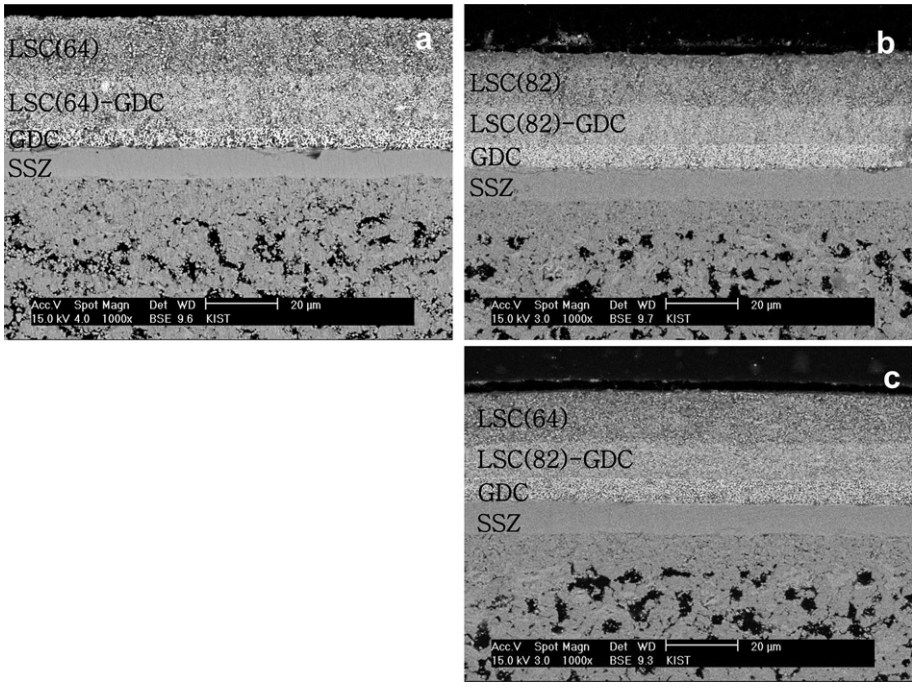

Fig. 5. Cross-sectional SEM images of 10 × 10 cm^2 (a) LSC6464, (b) LSC8282, and (c) LSC8264 unit cells.

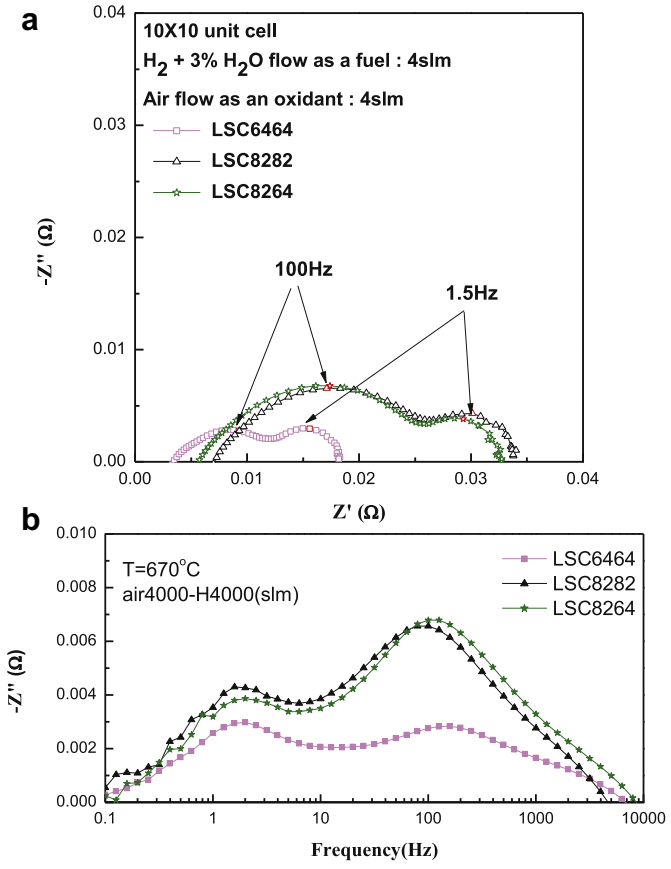

Fig. 7. Comparison of (a) Nyquist and (b) Bode plots for three differently configured 10×10 cm^2 LSC-based cathode unit cells (670 °C).

a hybrid of high current-collecting efficiency from the LSC64-based CCCL with the less electrochemically active LSC82-based CFL. These interpretations were supported by the results of the AC impedance analysis, as shown in Fig. 7.

As like in the previous results (Fig. 4), the IS for all the unit cells shown in Fig. 7 also consist of two impedance arcs: a large high-frequency impedance arc ($f_{peak} \approx 100$ Hz) and a smaller low-frequency impedance arc ($f_{peak} \approx 1.5$ Hz). Since the low-frequency component originated from the anode rather than from the cathode, as we previously demonstrated, we only considered the high-frequency component for our interpretation. Among the cells, the LSC6464 cell showed the smallest ohmic and polarization resistance compared with LSC8282 and LSC8264 cells because of the high electrochemical activity and current-collecting efficiency of the LSC64-based cathode material. This result implies that using the conductive LSC64-based CCCL instead of the LSC82-based CCCL reduced the amount of interfacial contact resistance between the cathode and the metallic interconnector while maintaining a similar level of cathode polarization resistance, thereby generating mid-level LSC8264 cell performance.

4. Conclusion

In the present study, the $La_{0.6}Sr_{0.4}CoO_3$ (LSC64) material composition was more effective than the $La_{0.8}Sr_{0.2}CoO_3$ (LSC82) one for increasing both the electrocatalytic activation of the cathode and the current-collecting efficiency between the cathode and the interconnect. The high electrical conductivity of LSC64 resulted in superior in current-collecting efficiency, which in turn resulted in a decreased ohmic polarization loss in unit cells. Moreover, electrocatalytically active LSC64 was a more appropriate material for a cathode functional layer to reduce the activation polarization in the cathode. The effectively controlled current-collecting layer increased unit-cell performance very efficiently by reducing the amount of ohmic and polarization losses in the SOFC cathode.

Acknowledgments

This work was supported by the Fundamental Research and Development Program for Core Technology of Materials, funded by the Ministry of Knowledge Economy, Republic of Korea and by the Institutional Research Program of the Korea Institute of Science and Technology (KIST).

References

[1] E. Ivers-Tiffée, A. Weber, D. Herbstritt, J. Eur. Ceramic Soc. 21 (10–11) (2001) 1805.
[2] S.P. Jiang, J. Mater. Sci. 43 (21) (2008) 6799.
[3] W. Wang, M. Mogensen, Solid State Ionics 176 (5–6) (2005) 457.
[4] C.W. Sun, R. Hui, J. Roller, J. Solid State Electrochem. 14 (7) (2010) 1125.
[5] N.Q. Minh, Ecs Trans. 25 (2) (2009) 241.
[6] T. Inoue, K. Eguchi, T. Setoguchi, H. Arai, Solid State Ionics 40-41 (1) (1990) 407.
[7] E. Siebert, A. Hammouche, M. Kleitz, Electrochim. Acta 40 (11) (1995) 1741.
[8] S.B. Adler, Chem. Rev. 104 (2004) 4791.
[9] A.J. McEvoy, Solid State Ionics 135 (1–4) (2000) 331.
[10] P.M. Raccah, J.B. Goodenough, Phys. Rev. 155 (3) (1967) 932.
[11] M.A. Señarís-Rodríguez, J.B. Goodenough, J. Solid State Chem. 116 (2) (1995) 224.
[12] T. Nakamura, M. Misono, Y. Yoneda, J. Catal. 83 (1) (1983) 151.
[13] K. Tabata, S. Kohiki, J. Mater. Sci. 23 (3) (1988) 1056.
[14] O. Yamamoto, Y. Takeda, R. Kanno, M. Noda, Solid State Ionics 22 (2–3) (1987) 241.
[15] M.H.R. Lankhorst, H.J.M. Bouwmeester, H. Verweij, Solid State Ionics 96 (1–2) (1997) 21.
[16] A. Weber, E. Ivers-Tiffee, J. Power Sources 127 (1–2) (2004) 273.
[17] M. Shiono, K. Kobayashi, T.L. Nguyen, K. Hosoda, T. Kato, K. Ota, M. Dokiya, Solid State Ionics 170 (1–2) (2004) 1.
[18] C. Rossignol, J.M. Ralph, J.M. Bae, J.T. Vaughey, Solid State Ionics 175 (1–4) (2004) 59.
[19] S.B. Adler, Solid State Ionics 111 (10) (1998) 125.
[20] T. Bak, J. Nowotny, M. Rekas, S. Ringer, C. Sorrell, Ionics 7 (4) (2001) 360.
[21] J. Mizusaki, Y. Mima, S. Yamauchi, K. Fueki, H. Tagawa, J. Solid State Chem. 80 (1) (1989) 102.
[22] H. Ullmann, N. Trofimenko, F. Tietz, D. Stöver, A. Ahmad-Khanlou, Solid State Ionics 138 (1–2) (2000) 79.
[23] D. Baskar, S.B. Adler, Chem. Mater. 20 (8) (2008) 2624.
[24] F. Tietz, Ionics 5 (1999) 129.
[25] H.Y. Jung, S.H. Choi, H. Kim, J.W. Son, J. Kim, H.W. Lee, J.H. Lee, J. Power Sources 159 (1) (2006) 478.
[26] C.H. Zhao, R.Z. Liu, L. Shao, S.R. Wang, T.L. Wen, J. Alloy Compd. 496 (1–2) (2010) 433.
[27] Y. Tao, H. Nishino, S. Ashidate, H. Kokubo, M. Watanabe, H. Uchida, Electrochim. Acta 54 (12) (2009) 3309.
[28] T.S. Zhang, J. Ma, J. Chan, J.A. Kilner, Solid State Ionics 176 (3–4) (2005) 377.
[29] J. Fleig, Annu. Rev. Mater. Res. 33 (2003) 361.
[30] A. Endo, S. Wada, C.J. Wen, H. Komiyama, K. Yamada, J. Electrochem. Soc. 145 (3) (1998) L35.
[31] T. Horita, K. Yamaji, N. Sakai, H. Yokokawa, A. Weber, E. Ivers-Tiffée, Electrochim. Acta 46 (12) (2001) 1837.
[32] R.A. De Souza, J.A. Kilner, Solid State Ionics 126 (1–2) (1999) 153.
[33] Y. Lu, C. Kreller, S.B. Adler, J. Electrochem. Soc. 156 (4) (2009) B513.
[34] N. Bonanos, B.C.H. Steele, E.P. Butler, Impedance Spectroscopy, John Wiley & Sons, Inc, 2005, pp. 205–537.
[35] A. Bieberle-Hutter, L.P. Meier, L.J. Gauckler, J. Electrochem. Soc. 148 (6) (2001) A646.
[36] Y.L. Yang, A.J. Jacobson, C.L. Chen, G.P. Luo, K.D. Ross, C.W. Chu, Appl. Phys. Lett. 79 (6) (2001) 776.
[37] S.B. Adler, Solid State Ionics 111 (1–2) (1998) 125.
[38] J. Hwang, H. Lee, K.J. Yoon, H.W. Lee, B.K. Kim, J.H. Lee, J.W. Son, J. Electrochem. Soc. 159 (10) (2012) F639.
[39] J.A. Kilner, R.A. De Souza, I.C. Fullarton, Solid State Ionics 86–88 (2) (1996) 703.